Ultrasound elastography to quantify average percent pressure-normalized strain reduction associated with different aortic endografts in 3D-printed hydrogel phantoms

Dakota W. Gonring, BA,[a] Zachary R. Zottola, BS,[a] Adnan A. Hirad, MD, PhD,[b] Ronald Lakony, BS,[c] Michael S. Richards, PhD,[d] Grayson Pitcher, MD,[b] Michael C. Stoner, MD,[b] and Doran S. Mix, MD,[b] *Rochester, NY*

ABSTRACT

Objective: Strain has become a viable index for evaluating abdominal aortic aneurysm stability after endovascular aneurysm repair (EVAR). In addition, literature has shown that healthy aortic tissue requires a degree of strain to maintain homeostasis. This has led to the hypothesis that too much strain reduction conferred by a high degree of graft oversizing is detrimental to the aneurysm neck in the seal zone of abdominal aortic aneurysms after EVAR. We investigated this in a laboratory experiment by examining the effects that graft oversizing has on the pressure-normalized strain ($\overline{\varepsilon_{\rho+}}$/pulse pressure [PP]) reduction using four different infrarenal EVAR endografts and our ultrasound elastography technique. Approximate graft oversizing percentages were 20% (30 mm phantom-graft combinations), 30% (28 mm phantom-graft combinations), and 50% (24 mm phantom-graft combinations).

Methods: Axisymmetric, 10% by mass polyvinyl alcohol phantoms were connected to a flow simulator. Ultrasound elastography was performed before and after implantation with the four different endografts: (1) 36 mm polyester/ stainless steel, (2) 36 mm polyester/electropolished nitinol, (3) 35 mm polytetrafluoroethylene (PTFE)/nitinol, and (4) 36 mm nitinol/polyester/platinum-iridium. Five ultrasound cine loops were taken of each phantom-graft combination. They were analyzed over two different cardiac cycles (end-diastole to end-diastole), yielding a total of 10 maximum mean principal strain ($\overline{\varepsilon_{\rho+}}$) values. $\overline{\varepsilon_{\rho+}}$ was divided by pulse pressure to yield pressure-normalized strain ($\overline{\varepsilon_{\rho+}}$/PP). An analysis of variance was performed for graft comparisons. We calculated the average percent $\overline{\varepsilon_{\rho+}}$/PP reduction by manufacturer and percent oversizing. These values were used for linear regression analysis.

Results: Results from one-way analysis of variance showed a significant difference in $\overline{\varepsilon_{\rho+}}$/PP between the empty phantom condition and all oversizing conditions for all graft manufacturers (F(3, 56) = 106.7 [graft A], 132.7 [graft B], 106.5 [graft C], 105.7 [graft D], $P < .0001$ for grafts A-D). There was a significant difference when comparing the 50% condition with the 30% and 20% conditions across all manufacturers by post hoc analysis ($P < .0001$). No significant difference was found when comparing the 20% and 30% oversizing conditions for any of the manufacturers or when comparing $\overline{\varepsilon_{\rho+}}$/PP values across the manufacturers according to percent oversize. Linear regression demonstrated a significant positive correlation between the percent graft oversize and the all-graft average percent $\overline{\varepsilon_{\rho+}}$/PP reduction ($R^2 = 0.84$, $P < .0001$).

Conclusions: This brief report suggests that a 10% increase in graft oversizing leads to an approximate 5.9% reduction in $\overline{\varepsilon_{\rho+}}$/PP on average. Applied clinically, this increase may result in increased stiffness in axisymmetric vessels after EVAR. Further research is needed to determine if this is clinically significant. (JVS—Vascular Science 2024;5:100198.)

Clinical Relevance: This research suggests that a higher degree of graft oversizing results in a higher average percent pressure-normalized strain reduction and thus increased mechanical stiffness. There is evidence suggesting that arteries become less pulsatile when they become stiffened. Therefore, decreasing aortic pulsatile flow by implanting a highly oversized graft may have deleterious long-term effects after endovascular aneurysm repair. This may have implications for future graft construction and for the choice of endograft by the surgeon, especially when considering the benefits of strain reduction to the diseased tissue that comprises the aneurysmal sac. In addition, our technique allows for the assessment of dynamic changes to stiffness after graft implantation in vivo.

Keywords: Abdominal aortic aneurysm; Ultrasound elastography; Endovascular aneurysm repair; Graft oversizing

---

In recent years, graft technology has become increasingly sophisticated, allowing for endovascular aneurysm repair (EVAR) to be performed in a growing percentage of patients with complex anatomy.[1-3] Specifically, many of these patients have adverse aneurysmal neck characteristics, including those that are large in diameter, short in length, and have a high degree of angulation.[4-6] Such patients typically fall outside of the endograft manufacturer's instructions for use (IFU) criteria, which places them at increased risk for late proximal (type 1A) endoleaks and higher aneurysm-related mortality.[7,8] Late type 1A endoleaks are among the most consequential post-EVAR complications as they tend to repressurize the atrophied sac, leading to sac enlargement and potentially aortic rupture.[7,9,10] It is theorized that these endoleaks develop due to graft migration and proximal neck degeneration, especially when graft oversizing is beyond 30%, but this finding is controversial and remains poorly studied.[7,11,12] The relationship between neck characteristics, IFU specifications, and graft failure modes has been established in the literature, but the factors that lead to the natural progression of these events have been incompletely explored.

One index that has been increasingly used to evaluate abdominal aortic aneurysms (AAAs) after EVAR is biomechanical stiffness. By examining pressure-normalized strain, previous studies have demonstrated an inverse relationship between aneurysmal sac stiffness and rupture risk, that is, that increased stiffness is associated with increased aneurysm sac stability.[13-15] Our group recently conducted a related study examining the biomechanics of the aneurysm sac immediately before and after EVAR. We observed an increase in stiffness at the sac-graft interface via a decrease in pressure-normalized strain ($\overline{\varepsilon_{\rho+}}$/pulse pressure [PP]), thus demonstrating the benefit of endograft implantation to the diseased tissue of the aneurysm on a biomechanical level.[16] Unfortunately, it is largely unknown how these same principles apply to the neck after EVAR, but additional findings in the literature can help us develop an informed hypothesis. In previous studies, it has been reported that when healthy tissue becomes stiffened, cardiovascular and all-cause mortality both increase.[17] Less compliant blood vessels are associated with arterial dysfunction and the development of vascular pathology.[18,19] Furthermore, pathologic cardiac remodeling has been observed after endovascular repair of descending thoracic aortic aneurysms, due to stiffness discordance between the implanted endograft and the underlying native tissue.[20] These notions suggest that physiologically maintained compliance is required for the long-term preservation of cardiovascular tissue. Therefore, we postulate that increased stiffness conferred by excessive graft oversizing in the neck of AAAs after EVAR is potentially detrimental to healthy aortic wall

ARTICLE HIGHLIGHTS

- **Type of Research**: Brief report
- **Key Findings:** Using our ultrasound elastography technique, we observed that a higher degree of graft oversizing is associated with an increased average percent strain reduction when deploying four different endovascular aneurysm repair endografts inside 3D-printed hydrogel phantoms measuring 24, 28, and 30 mm in diameter. The coefficient of determination (R^2) from the linear regression of the all-graft average percent pressure-normalized strain reduction was 0.84 ($P < .0001$). This regression suggests that pressure-normalized strain will reduce by approximately 5.9% for every 10% increase in graft oversize.
- **Take Home Message:** Our simulation study suggests that commercially available endografts produce similar reductions in principal strain. This reduction is linear between 20% and 50% oversizing.

function and may lead to further aneurysmal degeneration, even though increased stiffness in the EVAR-sac construct itself is beneficial.

To test this hypothesis, we devised an experimental model to examine the biomechanical effects that various endografts and oversizing might have on the neck of AAAs. We 3D-printed axisymmetric tissue-mimicking phantom hydrogel vessels from polyvinyl alcohol cryogel (PVA-c), a material that has previously been biologically validated against vascular tissue.[21,22] Our fabricated vessels measured 30 mm, 28 mm, and 24 mm in diameter. We implanted our vessels with four different EVAR grafts and connected them to a cardiac flow simulator. Graft compositions were polyester/stainless steel at 36 mm in diameter (1), polyester/electropolished nitinol at 36 mm in diameter (2), PTFE/nitinol at 35 mm in diameter (3), and nitinol/polyester/platinum-iridium at 36 mm in diameter (4). Percent oversizing ranged from 20% to 50% for grafts A, B, and D, whereas percent oversizing ranged from 17% to 46% for graft C. For simplicity, we refer to the three oversizing conditions as approximately 20%, 30%, and 50% across all graft manufacturers. Using ultrasound elastography, we measured the $\overline{\varepsilon_{\rho+}}$/PP associated with each trial. $\overline{\varepsilon_{\rho+}}$/PP is inversely proportional to modulus, a mathematical descriptor of stiffness.[23] Finally, we looked to the literature to determine if our findings had any potential biologic implications for aneurysmal necks after EVAR.

METHODS

Phantom vessel construction. All 3D prints were designed using MeshMixer version 3.5 opensource Autodesk software. Molds were designed to yield

axisymmetric tubes 304.8 mm (12 inches) in length with 5 mm wall thickness. We chose to manufacture our phantoms with slightly thicker walls than the human aorta to withstand repeated mechanical manipulation and from prior experience in reproducing hydrogels. It is important to note that our previous work showed a 4% to 6% principal strain in our phantoms with a PP of 20 to 100 mm Hg, which is what would be expected for the human aorta.[23] Therefore, from a mechanics standpoint, our model mimics human aortic displacements, independent of wall thickness, across a range of PPs, including those that are physiologic. Phantom wall thickness was preserved between each of the phantoms so that results could be compared reliably. Our three vessel-mimicking phantoms had inner diameters measuring 24, 28, and 30 mm. Stereolithography (.stl) files of all molds were printed using the Raise3D Pro2 Plus 3D printer and Raise3D premium polylactic acid filament. End connectors had one path for flow with an outer diameter corresponding to the inner diameter of the phantom. The outflow tract had an external diameter of 12.7 mm (0.5 inches) and barbs to prevent tube slippage. End connectors were created using the Stratasys J750 printer.

Batches of homogeneous 10% w/v PVA solution were made in a similar fashion to established protocols in the literature.[22,24] Mold phantom structures were frozen for 12 hours and then allowed to thaw for 12 hours for a total of 5 freeze-thaw cycles. After the fifth and final thaw, phantoms were carefully removed from their molds using tap water. Phantoms were stored in a sealed container with a 5% by volume bleach/water solution at room temperature.

We also created two axisymmetric, cylindrical background phantoms. Given the tolerance of the experiment, we used one large background for the 28- and 30-mm phantoms and a separate one for the 24-mm phantom. These backgrounds were designed to slide over their respective phantom vessels to mimic retroperitoneal tissue and provide mechanical stability.[22] Background molds were created using the same software, printer, and filament as those used in creating phantom vessels. The outer diameters and heights of the backgrounds measured 18.5 cm and 13.5 cm, respectively. 3D-printed cylinders for background lumens measured 36 mm (for the 30 mm and 28 mm vessels) and 32 mm (for the 24 mm vessel). Batches of background solution were created by microwaving 35 g of PVA in 700 mL of water (5% w/v) in a covered container until translucent. The solution was then allowed to cool to room temperature in a water bath before stirring in 1.4 g of calcium carbonate (0.2% w/v) suspended in 10 mL of water. Backgrounds were subjected to 5 freeze-thaw cycles. Given the increased volume of PVA, freeze-thaw cycles were increased to 48 hours.

Graft selection and degassing process. To investigate the pressure-normalized strain conferred by various commercially available grafts, we chose to maintain graft size while serially decreasing phantom vessel size. We aimed to have a minimum degree of oversizing within the 10% to 20% range traditionally recommended clinically.[25] To achieve this in our largest phantom vessel (30 mm), grafts could be no larger than 36 mm. Graft compositions were polyester/stainless steel at 36 mm in diameter (1), polyester/electropolished nitinol at 36 mm in diameter (2), PTFE/nitinol at 35 mm in diameter (3), and nitinol/polyester/platinum-iridium at 36 mm in diameter (4). Ideally, grafts would have had the same diameter, but the graft C manufacturer did not have a 36 mm device when we conducted our study. We still found it appropriate to include it in our investigation because it was in the 10% to 20% range, and the 1 mm difference likely would not drastically affect clinical decision-making. All grafts were degassed under negative pressure for 7 days before implantation to optimize acoustic properties.

Experimental methods. Tubing was placed through both sides of the long end of a 30-gallon plastic tub and made watertight so it could be connected to the rest of the circuit. Tubing was placed 7.5 cm from the bottom of the tub.

One of each graft was implanted into the three phantoms and was used for all experiments. Percent oversizing ranged from 20% to 50% for grafts A, B, and D, whereas percent oversizing ranged from 17% to 46% for graft C. Percent oversize was calculated as the difference between the phantom vessel diameter, before implantation, and the diameter of each graft, normalized by the diameter of the phantom. The resulting value was then multiplied by 100 to yield a percent. Vessel phantoms were placed in the background phantoms, and the combined phantoms were attached to the tubes in a water bath. The barbed ends of the 3D-printed end connectors matching the phantom to be used were connected to tubing inside of the tub. Circumferential clamps were placed outside of the phantoms to ensure an adequate seal. To load a phantom with an endograft, phantoms first had to be rolled down halfway to expose their inner wall. The EVAR graft legs were then placed in contact with the inside-out portion of the lumen before being rolled back up with the main body of the graft situated in the middle. Endografts were placed in the middle of each of the phantoms, so the main body, approximately 50 mm, was 25 mm from the inlet of the flow simulator to prevent changes to strain that might be imparted by the flow loop itself. To ensure an adequate radial seal and create an idealized graft-phantom interface, we dilated with a Q50 stent graft balloon (Merit Medical) for 2 minutes before connecting graft-phantom pairs to the flow simulator. This same graft-wall interface was
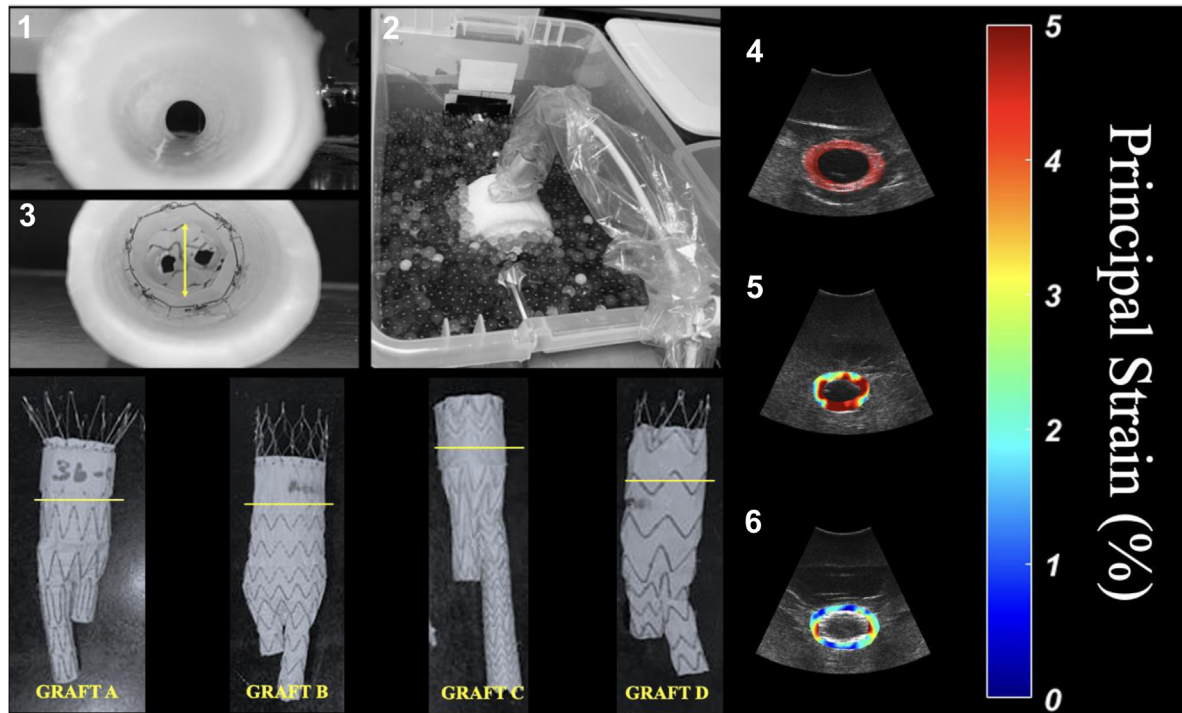
Fig 1. Experimental methods and materials used. **A,** Empty phantom vessel condition. **B,** Phantom-background combination connected to the flow simulator with the ultrasound probe placed on the background for image collection, **C,** Graft implantation in a 28 mm phantom vessel with the yellow arrow annotating the region of measurement. Image processing can be seen in **(D)**-**(F)**. **D,** Finite element mesh overlaying B-mode ultrasound of 24 mm phantom without endograft. **E,** Resulting parametric imaging showing peak mean principal strain. **F,** Parametric imaging of 24 mm phantom with graft B inserted for comparison. The color scale to the right of **(F)** shows relative values that correspond to the degree of strain as demonstrated on parametric imaging over the cardiac cycle. Grafts A-D used in the experiment are also displayed with the yellow lines demonstrating approximate locations for data collection.

established between oversizing conditions. One of each type of graft was implanted into the three phantoms and was used for all experiments. Data replicates were done in the same phantom model per study group. Grafts were removed by gently rolling phantoms inside out, plus gentle traction provided by Debackey forceps. Water absorbing beads (Notchis Colorful Water Gel Beads, Amazon) were placed in the water bath for additional phantom support and to improve acoustic conditions (Fig 1).

Water was pumped through the phantom using a Vivitro SuperPump cardiac simulator. The pump was driven by a preinstalled waveform, Physio_70, which has a duty cycle of 35%, a pump rate of 1.17 Hz or 70 BPM, and produces physiologic pulsatile flow. We first established an average flow of approximately 3.5 L/min to operate our system. Two inline Transonic ME 13 PXN flow probes monitored flow, with one placed proximally and one distally. Flow was measured using a Transonic TS410 flow meter, which output analog pressure readings to a data acquisition system (DAQ National instruments USB-6005) for recording. The distal resistance dial modulated the average pressure in the circuit. Refinements in

PP were made by adjusting the air-fluid ratio of the compliance chambers. Pressure was detected by a single Millar Mikro-Cath pressure probe placed directly inside of the phantom during the trial. Tests were performed at a maximum pressure of approximately 40 mm Hg and PPs of approximately 35 mm Hg across all conditions. A heater was placed in the loop to heat circulating fluid to $37.8\,^{\circ}\mathrm{C}\ (100\,^{\circ}\mathrm{F})$ to mimic heat-related effects at body temperature.

Transverse plane images of the main body of each graft were collected with the Ultrasonix Sonix-Touch US System (Anologic OS) and the Ultrasonix C7-3/50 convex transducer. Image quality was optimized by adjusting sector, depth, and gain. Images were recorded at a frequency of 5 MHz with standard B-mode ultrasound (US image. The US image plane was held in place approximately 25 mm distal to the proximal ends of each graft, and five successive US cine loops were recorded in the exact location at the graft-phantom interface.

Radiofrequency US image sequences from each cine loop were uploaded to MATLAB (Mathworks) for strain analysis as described in our previous work.[16] PP values were manually recorded during each trial.
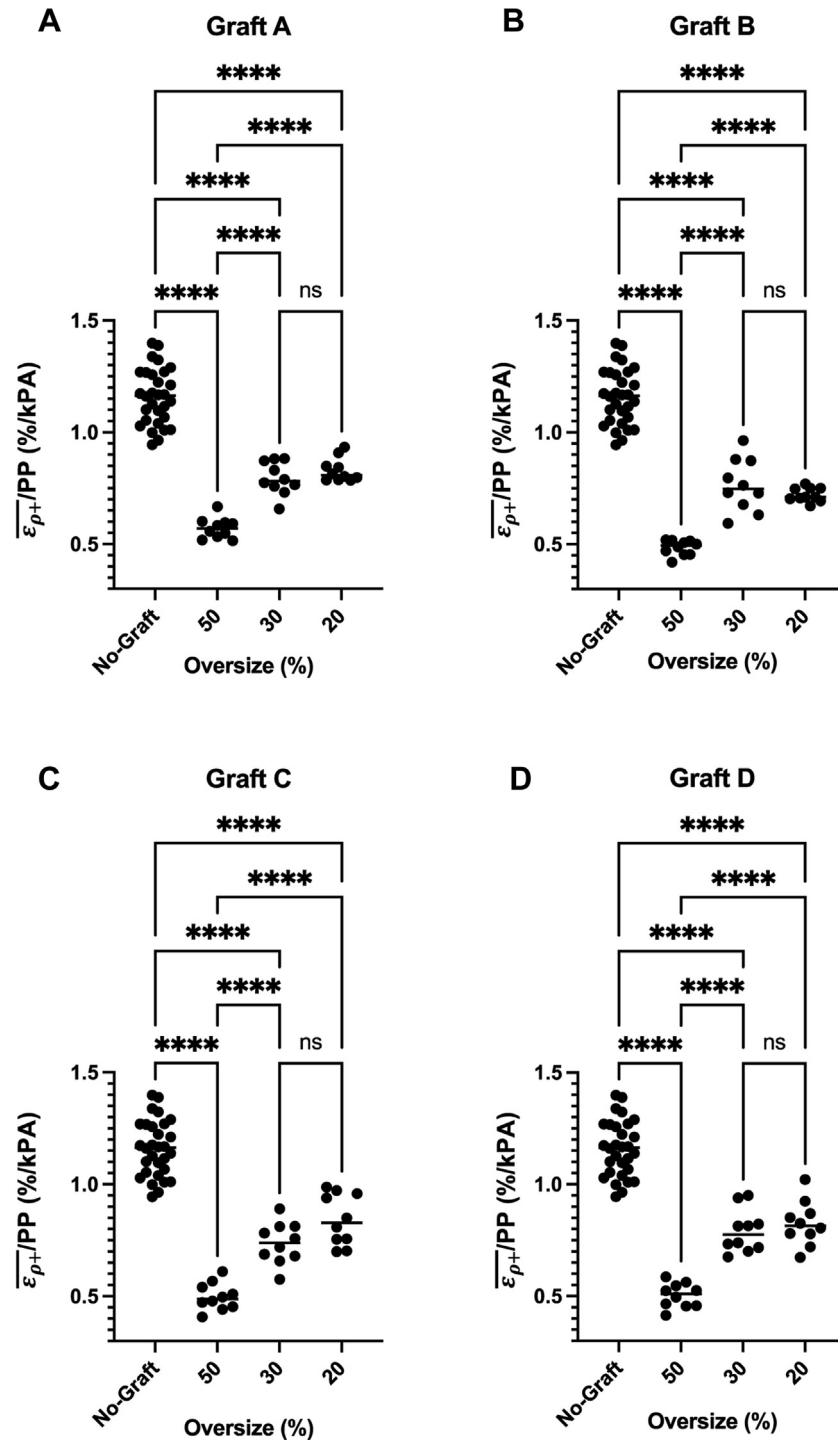
Fig 2. Raw dataset of pressure-normalized strain values associated with each graft manufacturer. Results of analysis of variance are shown above each bracket indicating the compared conditions. The asterisks above the brackets represent a significant result, whereas "ns" denotes a nonsignificant result. Across all graft manufacturers, there was a significant difference between the empty phantom condition and all oversizing conditions. There was also a significant difference when comparing the 50% condition with the 30% and 20% conditions across all manufacturers. In addition, there was no significant difference when comparing the 20% and 30% oversizing conditions for any of the manufacturers. Graft compositions were polyester/stainless steel 36 mm in diameter **(A)**, polyester/electropolished nitinol 36 mm in diameter **(B)**, PTFE/nitinol 35 mm in diameter **(C)**, and nitinol/polyester/platinum-iridium 36 mm in diameter **(D)**. Phantom vessel sizes were 24, 28, and 30 mm in diameter. *PTFE*, polytetrafluoroethylene; *PP*, Pulse pressure.
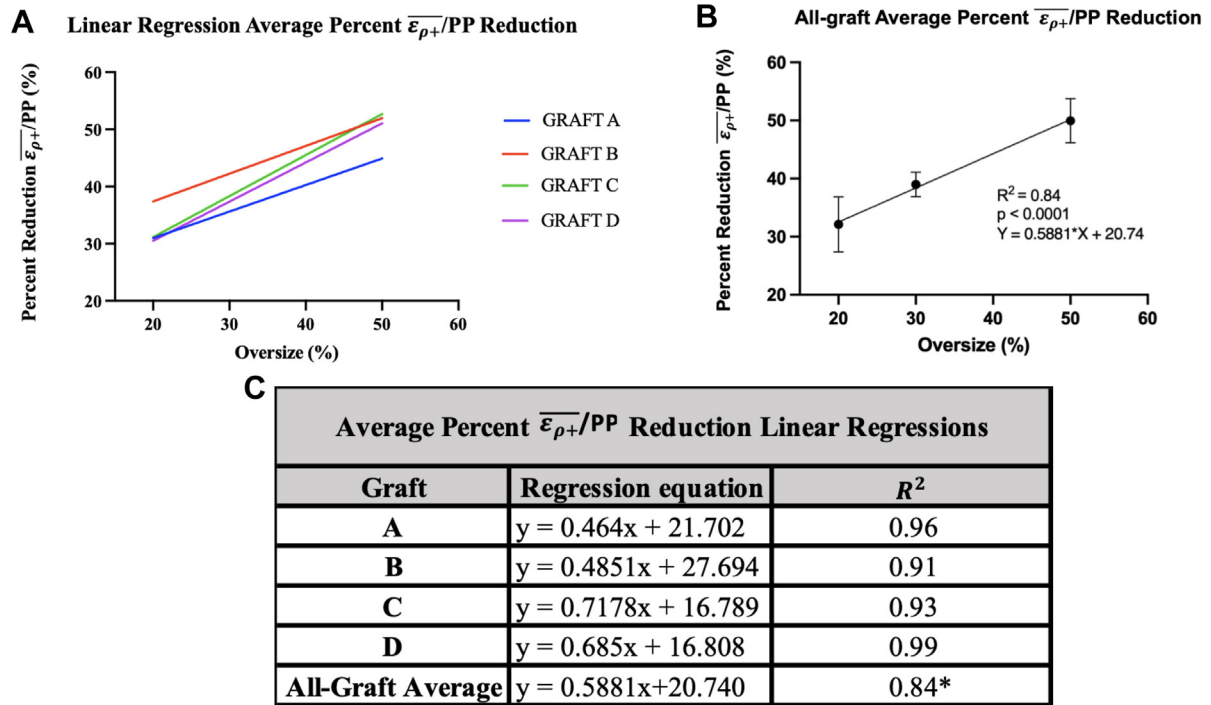
Fig 3. A, Linear regression associated with the four individual grafts. **B,** The all-graft average percent pressure-normalized strain reduction. Exact values used can be seen in Table II. **C,** Equations associated with the linear regressions for grafts A-D and the all-graft average. Coefficients of determination are also included with asterisks to indicate statistical significance ($P < .0001$). *PP,* Pulse pressure.

Image processing and data analysis. For each captured cine loop, two independent observers on the study team selected frames over one simulated cardiac cycle (end-diastole to end-diastole), defined as the point where the phantom luminal area was minimized. Each observer then used our MATLAB code to select a region of interest between the inner and outer vessel walls for strain analysis. Our custom algorithm then overlayed a 2D finite element mesh on the region of interest to track the frame-by-frame displacement values on the finite element mesh. The resultant displacement vector field was then used to calculate 2D strain tensor fields, as described by our prior work.[23] Peak strain corresponding to the frame with the maximum mean principal strain ($\overline{\varepsilon_{\rho+}}$) was divided by the PP associated with the trial to yield $\overline{\varepsilon_{\rho+}}$/PP. Finally, a parametric image of this frame depicting instantaneous relative regional strain was generated (Fig 1), similar to methods in other studies.[23,26] A total of 75 independent tests were performed yielding 75 pressure-normalized strain reduction values. $\overline{\varepsilon_{\rho+}}$/PP in each trial was averaged according to manufacturer and phantom size. One-way analysis of variance testing and post hoc analysis with Tukey's honestly significant difference were performed for intragraft comparisons (Fig 2). The average percent $\overline{\varepsilon_{\rho+}}$/PP reduction was calculated according to the manufacturer for each oversize condition. To calculate average percent pressure-

normalized strain reduction, the average pressure-normalized strain of the oversized condition associated with a manufacturer was subtracted from the average pressure-normalized strain of the corresponding empty-phantom condition. The difference between these values was then divided by the same average pressure-normalized strain associated with the empty phantom and the result was multiplied by 100 to yield a percent. These values were used for linear regression and to compute an all-graft average for linear regression with corresponding coefficients of determination (R^2) (Fig 3).

RESULTS

Interobserver reliability. The degree of concordance between the two recorded observer values for each trial was determined by a two-way intraclass correlation coefficient (ICC). The calculated ICC indicates high concordance between observer values (ICC = 0.94, 95% confidence interval: 0.91-0.96, n = 75).

Graft comparisons by analysis of variance analysis. Across all graft manufacturers, there was a significant difference between the empty phantom condition and all oversizing conditions as demonstrated in Fig 2 ($F_{(3, 56)}$ = 106.7 [graft A], 132.7 [graft B], 106.5 [graft C], 105.7 [graft D], $P < .0001$ for grafts A-D). To further evaluate intergroup differences across the oversizing conditions

Table I. Average pressure-normalized strain by manufacturer and approximate percent oversize with no-graft values for comparison

Approximate percent oversize, %	Average pressure-normalized strain values (%/kPA), mean ± SD				
	Graft A	Graft B	Graft C	Graft D	No graft
20	0.83 ± 0.05	0.72 ± 0.03	0.84 ± 0.11	0.83 ± 0.10	1.19 ± 0.08
30	0.79 ± 0.07	0.76 ± 0.12	0.74 ± 0.09	0.79 ± 0.10	1.26 ± 0.09
50	0.57 ± 0.05	0.48 ± 0.03	0.50 ± 0.06	0.50 ± 0.05	1.03 ± 0.05

SD, Standard deviation.

for each of the grafts, post hoc comparisons were conducted using Tukey's honestly significant difference test (Fig 2). Post hoc analysis demonstrated a significant difference when comparing the 50% condition with the 30% and 20% conditions across all manufacturers ($P <$ .0001). No significant differences were found when comparing 20% to 30% oversizing. There was also no significant difference in $\overline{\varepsilon_{\rho+}}$/PP between graft manufacturers across the individual oversizing conditions.

Average percent $\overline{\varepsilon_{\rho+}}$/PP reduction. Ten $\overline{\varepsilon_{\rho+}}$/PP values were calculated for each graft per phantom using the five US cine loops. Mean $\overline{\varepsilon_{\rho+}}$/PP values associated with each of the oversizing conditions (Table I) were used to calculate the average $\overline{\varepsilon_{\rho+}}$/PP reduction. The greatest reduction in $\overline{\varepsilon_{\rho+}}$/PP was observed in the 24 mm phantom in all grafts. All graft compositions had a positive, statistically nonsignificant, correlation associated with the percent $\overline{\varepsilon_{\rho+}}$/PP reduction vs percent oversizing (Fig 3). The mean of the average percent reductions across all oversizing conditions was plotted and showed a significant, positive correlation with percent oversizing ($R^2 =$ 0.84, $P <$ .0001) and suggests that, on average, $\overline{\varepsilon_{\rho+}}$/PP will be reduced by approximately 0.59% for every percent increase in graft oversize.

DISCUSSION

Although EVAR has become the preferred method for surgically treating AAAs, long-term durability of EVAR continues to be a serious concern, as up to 30% of these patients will require secondary intervention after 10 years.[1,27] The causes of reintervention arising from aneurysmal neck pathology are among the most significant, including neck dilation, type 1 endoleak, and graft migration.[28] Rupture, perhaps the most devastating consequence of graft failure, is most often caused by endoleak with the highest proportion of cases arising from proximal (type 1A) seal failures.[29] Clearly, the proximal aneurysm neck plays a vital role in influencing treatment outcomes. Unfortunately, the factors that benefit or harm the neck are not fully understood. Although controversial, the degree of graft oversizing is one factor implicated in aneurysmal neck degeneration and proximal seal failure. In a prospective study on a small group

of patients treated with Ancure endografts (Guidant) oversized by 2 to 4 mm, Prinssen et al[30] observed a continuous, linear increase of approximately 1 mm/y in diameter at the graft wall interface over 2 (N = 27) and 3 (N = 13) years. The Ancure—composed of unsupported woven polyester—was removed from the market in 2003, so it is unclear how these findings impact our understanding of the effects of oversizing in the present study, but they may shed light on how graft technology itself plays a role in influencing treatment outcomes. Monahan et al[31] conducted a similar study examining neck dilation in patients (N = 46) who received EVAR with the Zenith endograft (Cook). Although they did observe a positive correlation between proximal neck dilation and percent oversizing, they found that neck dilatation developed fastest during early follow-up but was limited by endograft size and was not significantly associated with type 1 endoleak or graft migration. These findings are supported by other studies in the literature that made similar conclusions.[32-34] The direct impact of oversizing on endoleak and migration is also inconclusive. Some graft oversizing is necessary to achieve the radial force required for an adequate seal. Most graft IFUs recommend oversizing between 10% and 20%.[25] One study that was a part of the EUROSTAR registry found that the risk of endoleak decreased when endografts were oversized by 10% and up to 25%, especially in patients with favorable neck anatomy.[35] A high degree of oversizing however may increase the risk for adverse outcomes. Sternbergh et al[12] examined the effect of graft oversizing on endoleak and migration in 351 patients who received the Zenith AAA endograft. They found that graft oversizing beyond 30% resulted in a 14-fold increase in graft migration (>5 mm) at 1 year and was associated with a 16-fold increased risk of sac expansion at 2 years. Interestingly, they did not detect a significantly increased risk in endoleak associated with a high degree of oversizing, potentially highlighting the importance of other factors like patient-specific anatomy and the tendency to oversize more generously when unfavorable anatomic conditions are present. Several other studies have found no significant link between oversizing and endoleak or migration.[36-39] Indeed, there is no consensus on the clinical impact of graft oversizing. These effects

Table II. Calculated values associated with the average percent pressure-normalized strain reduction by manufacturer and approximate percent oversize

Approximate percent oversize, %	Average percent pressure-normalized strain reductions (%)				
	Graft A	Graft B	Graft C	Graft D	All-graft average, mean ± SD
20	30.0	39.2	28.9	30.4	32.1 ± 4.7
30	37.2	39.6	41.7	37.5	39.0 ± 2.1
50	44.4	52.8	51.6	51.0	50.0 ± 3.8

SD, Standard deviation.
Values associated with grafts A, B, C, and D were averaged to produce the all-graft averages. All-graft averages were plotted with linear regression seen in Fig 3.

may be better elucidated by examining the biomechanics associated with graft implantation in a laboratory setting given the challenges of conducting a similar investigation clinically, which was the aim of the current study.

In an earlier study, our group examined the biomechanical changes imparted by EVAR endografts on the aneurysm sac. We observed that stiffness in the sac increased immediately after graft deployment via a decrease in pressure-normalized strain ($\overline{\varepsilon_{\rho+}}$/PP).[16] These findings led us to hypothesize that stiffness in the neck of aneurysms also increases after EVAR. We tested this hypothesis in a laboratory setting by implanting various commercially available endografts (A, B, C, and D) in hydrogel phantoms (24 mm, 28 mm, and 30 mm) and measured $\overline{\varepsilon_{\rho+}}$/PP using ultrasound elastography. Hydrogel phantoms were constructed as axisymmetric tubes to approximate idealized aneurysmal necks. In addition, we calculated the percent reduction in $\overline{\varepsilon_{\rho+}}$/PP associated with each trial before averaging these values for each graft per phantom size. We found that the percent reduction in average pressure-normalized strain increased as the degree of graft oversizing increased. At the most basic level, stent grafts can be thought of as springs. Based on Hook's law of springs, we approximated the reduction in $\overline{\varepsilon_{\rho+}}$/PP with linear regression. The all-graft average percent $\overline{\varepsilon_{\rho+}}$/PP reduction across graft manufacturers showed a considerable correlation between the degree of graft oversizing and stiffness reduction ($R^2 = 0.84$, $P < .0001$). This regression suggests that, on average, pressure-normalized strain will reduce by approximately 5.9% for every 10% increase in graft oversize. The linear relationship for each graft complements these findings (Fig 3). Although our measurements appeared to be linear, the nonlinear behavior of vessel tissue suggests that with more trials and more extreme degrees of oversizing, the relationship between the $\overline{\varepsilon_{\rho+}}$/PP reduction and graft oversizing may not be linear.

From a biomechanical perspective, increasing the stiffness of nonaneurysmal vascular tissue has been shown to have negative consequences. A systemic review and meta-analysis on the effects of arterial stiffness determined that an increase in stiffness corresponding to an increased pulse wave velocity of 1 m/s resulted in a 15% increase in both cardiovascular mortality and all-cause mortality.[17] They conclude that aortic pulse wave velocity (stiffness) is a strong predictor of future cardiovascular and mortality events. Similar studies have concluded that deviations from native arterial compliance lead to arterial dysfunction and vascular pathology.[18,19] Morris et al[18] conducted an experiment to examine the biomechanical effects that stent grafts have on native vessels. They concluded that substantial abdominal aortic stiffening after stent-graft implantation may impede blood flow and increase mechanical stress at the stent-artery interface. Furthermore, they recommend that future stent grafts incorporate a more compliant proximal side to better mimic native arterial compliance. A similar experiment on the effects of compliance mismatch between four commercially available grafts and the arterial wall found that grafts decrease aortic wall compliance after implantation. They further recommend a graft design that preserves aortic elastic recoil to reduce the risk of device-related complications.[19] Our current study may complement these findings, as we did observe a marked increase in stiffness with greater endograft oversizing, especially when comparing the 20% and 30% conditions with the 50% condition. On the basis of our results, we hypothesize that graft implantation results in increased prestrain at baseline (a diastolic correlate) compared with the empty vessel condition. This increase may be quantified by the average percent $\overline{\varepsilon_{\rho+}}$/PP reduction associated with each graft-phantom combination. This metric has the potential to quantify AAA stability after endograft deployment.

Experimental research has shown that changing levels of stress and strain on blood vessels can trigger remodeling and prompt vessel growth.[40] A study in rats showed that smooth muscle cell orientation within blood vessels is impacted by tensile strain that plays an important role in pathologic remodeling and physiologic blood vessel growth.[41] Stiffer vessels expand and contract to a lesser degree than healthy elastic vessels. Accordingly, stiffer

tissue can be described as less pulsatile than compliant tissue. This is an important observation because evidence suggests that pulsatile blood flow and compliant vessels are required to maintain proper biologic arterial function. For example, experimental research has demonstrated that nonpulsatile flow impacts the normal exchange of constituents between interstitial and lymphatic fluids, potentially leading to metabolic derangements like acidosis.[42] Pulsatile flow has also been shown to impact blood pressure control by indirectly activating baroreceptors through arterial wall stretching.[43] These findings suggest that baseline changes in biomechanical properties may result in deleterious biological, structural, and cellular changes, especially in cases of EVAR failure arising from neck pathology.

Limitations. The purpose of our study was to investigate how oversized EVAR graft main bodies mechanically affect vessel-like walls in an idealized experiment. Changes to the study design, however, could impact the outcome. A more anatomically accurate model might produce results that are more clinically translatable. However, in light of the question we were attempting to answer, we felt that an axisymmetric tube was a basic approximation for aneurysmal neck morphometry. This may also challenge our use of the term "seal zone" as our model did not include a distal bifurcation. However, we view the seal zone as fundamentally arising from the radial force that is required to prevent endoleak, which we did not observe in our experiment under US imaging. Although phantom geometries were meant to mimic idealized neck morphology, we recorded our measurements approximately 25 mm distal to the most proximal regions of each of the grafts that may extend outside the seal zone in conventional cases clinically. Given our need for a standard process and the uniformity in graft composition, we believe that these data can be used to infer trends about graft behaviors, especially when concerning axisymmetric vessels. In addition, our model vessel was 304.8 mm in length, which differs from traditional IFU criteria for neck length and may result in measurements that are inaccurate to in vivo stiffness changes after EVAR clinically. It is also possible that our results apply best to fusiform aneurysms given their similar geometries.

We are further limited in our ability to apply the results clinically, as in vivo stiffness measurements may differ according to patient-specific factors like vessel geometry, disease burden, and biology. Homogeneous phantoms that model healthy tissue are imperfect in their approximation of aneurysmal necks, as in vivo, they are likely not completely healthy. In future studies, it will be beneficial to manufacture stiffer vessels to better mimic the tissue that comprises aneurysmal necks in humans. In addition,

an experiment that tests oversizing conditions in the 10% to 30% range might confer more clinical translatability. However, we view our findings as an important step to understanding vessel biomechanics after EVAR that can be expanded on with a wider range of experimental conditions.

In addition, measurements were recorded in only one cross-sectional segment for each of the grafts per phantom. It is possible that there are measurably different $\overline{\varepsilon_{\rho+}}$/PP values along the lengths of each graft that we did not detect. It may also be beneficial in future experiments for all studied grafts to be of the same size, if possible. In our case, the effect of the 1 mm size difference between graft C and the other three grafts is unclear, as there was no statistical difference between grafts across any of the oversizing conditions. In addition, data replicates were performed in the same phantom model per study group, which does not account for potential differences in phantom mechanics associated with the manufacturing process. Despite these limitations, the findings of the current study provide foundational insights into the biomechanical effects imparted to axisymmetric vessels after EVAR.

CONCLUSIONS

This is a proof-of-concept study suggesting that a higher degree of graft oversizing leads to increased $\overline{\varepsilon_{\rho+}}$/PP reduction and, potentially, increased stiffness in axisymmetric vessels like the aneurysmal neck; this may contribute to the dysfunction of healthy aortic tissue after EVAR including pathologic remodeling, endoleak development, and graft migration. If our findings are clinically confirmed, they suggest that rational EVAR graft design may involve material compositions that allow strain preservation in the neck of aneurysms with decreased strain in the aneurysm sac. Our data also suggest that relatively small changes in graft oversizing (ie, 20% vs 30%) may not result in statistically significant differences, but it is unclear what effect this may have clinically. This adds to the growing body of literature showing the utility of strain analysis to evaluate AAA stability. Further research is needed to support these findings and determine whether they are clinically significant.

AUTHOR CONTRIBUTIONS

Conception and design: DG, MR, MS, DM
Analysis and interpretation: DG, ZZ, AH, GP, MS, DM
Data collection: DG, RL
Writing the article: DG, AH
Critical revision of the article: DG, ZZ, RL, MR, GP, MS, DM
Final approval of the article: DG, ZZ, AH, RL, MR, GP, MS, DM
Statistical analysis: DG, AH

DISCLOSURES
None.

REFERENCES

1. Dua A, Kuy S, Lee CJ, Upchurch GR, Desai SS. Epidemiology of aortic aneurysm repair in the United States from 2000 to 2010. *J Vasc Surg.* 2014;59:1512—1517.
2. Panthofer AM, Olson SL, Rademacher BL, et al. Anatomic eligibility for endovascular aneurysm repair preserved over 2 years of surveillance. *J Vasc Surg.* 2021;74:1527—1536.e1.
3. Mehta M, Valdés FE, Nolte T, et al. A pivotal clinical study to evaluate the safety and effectiveness of the ovation abdominal stent graft system investigators. One-year outcomes from an international study of the ovation abdominal stent graft system for endovascular aneurysm repair. *J Vasc Surg.* 2014;59:65—73.e1-3.
4. Jacobs CR, Scali ST, Khan T, et al. Endovascular aneurysm repair conversion is an increasingly common indication for open abdominal aortic aneurysm repair. *J Vasc Surg.* 2022;75:144—152.e1.
5. Aburahma AF, Campbell JE, Mousa AY, et al. Clinical outcomes for hostile versus favorable aortic neck anatomy in endovascular aortic aneurysm repair using modular devices. *J Vasc Surg.* 2011;54:13—21.
6. Stather PW, Wild JB, Sayers RD, Bown MJ, Choke E. Endovascular aortic aneurysm repair in patients with hostile neck anatomy. *J Endovasc Ther.* 2013;20:623—637.
7. O'Donnell TF, McElroy IE, Mohebali J, et al. Late type 1A endoleaks: associated factors, prognosis and management strategies. *Ann Vasc Surg.* 2022;80:273—282.
8. Abbruzzese TA, Kwolek CJ, Brewster DC, et al. Outcomes following endovascular abdominal aortic aneurysm repair (EVAR): an anatomic and device-specific analysis. *J Vasc Surg.* 2008;48:19—28.
9. Zacharias N, Warner CJ, Taggert JB, et al. Anatomic characteristics of abdominal aortic aneurysms presenting with delayed rupture after endovascular aneurysm repair. *J Vasc Surg.* 2016;64:1629—1632.
10. Harris PL, Vallabhaneni SR, Desgranges P, Becquemin JP, van Marrewijk C, Laheij RJ. Incidence and risk factors of late rupture, conversion, and death after endovascular repair of infrarenal aortic aneurysms: the EUROSTAR experience. European Collaborators on Stent/graft techniques for aortic aneurysm repair. *J Vasc Surg.* 2000;32:739—749.
11. Kratzberg JA, Golzarian J, Raghavan ML. Role of graft oversizing in the fixation strength of barbed endovascular grafts. *J Vasc Surg.* 2009;49:1543—1553.
12. Sternbergh WC, Money SR, Greenberg RK, Chuter TA, Zenith Investigators. Influence of endograft oversizing on device migration, endoleak, aneurysm shrinkage, and aortic neck dilation: results from the Zenith Multicenter Trial. *J Vasc Surg.* 2004;39:20—26.
13. Di Martino ES, Bohra A, Vande Geest JP, Gupta N, Makaroun MS, Vorp DA. Biomechanical properties of ruptured versus electively repaired abdominal aortic aneurysm wall tissue. *J Vasc Surg.* 2006;43:570—576. discussion: 576.
14. Wilson K, Bradbury A, Whyman M, et al. Relationship between abdominal aortic aneurysm wall compliance and clinical outcome: a preliminary analysis. *Eur J Vasc Endovasc Surg.* 1998;15:472—477.
15. Wilson KA, Lee AJ, Lee AJ, et al. The relationship between aortic wall distensibility and rupture of infrarenal abdominal aortic aneurysm. *J Vasc Surg.* 2003;37:112—117.
16. Zottola ZR, Gonring DW, Wang ML, et al. Changes in intraoperative aortic strain as detected by ultrasound elastography in patients following abdominal endovascular aneurysm repair. *J Vasc Surg Cases Innov Tech.* 2022;8:762—769.
17. Vlachopoulos C, Aznaouridis K, Stefanadis C. Prediction of cardiovascular events and all-cause mortality with arterial stiffness: a systematic review and meta-analysis. *J Am Coll Cardiol.* 2010;55:1318—1327.
18. Morris L, Stefanov F, McGloughlin T. Stent graft performance in the treatment of abdominal aortic aneurysms: the influence of compliance and geometry. *J Biomech.* 2013;46:383—395.
19. Morris L, Stefanov F, Hynes N, Diethrich EB, Sultan S. An experimental evaluation of device/arterial wall compliance mismatch for four stent-graft devices and a multi-layer flow modulator device for the treatment of abdominal aortic aneurysms. *Eur J Vasc Endovasc Surg.* 2016;51:44—55.
20. Van Bakel TMJ, Arthurs CJ, Nauta FJH, et al. Cardiac remodelling following thoracic endovascular aortic repair for descending aortic aneurysms. *Eur J Cardio Thorac Surg.* 2019;55:1061—1070.
21. Zell K, Sperl JI, Vogel MW, Niessner R, Haisch C. Acoustical properties of selected tissue phantom materials for ultrasound imaging. *Phys Med Biol.* 2007;52:N475—N484.
22. Mix DS, Stoner MC, Day SW, Richards MS. Manufacturing abdominal aorta hydrogel tissue-mimicking phantoms for ultrasound elastography validation. *J Vis Exp.* 2018;139:57984.
23. Mix DS, Yang L, Johnson CC, et al. Detecting regional stiffness changes in aortic aneurysmal geometries using pressure-normalized strain. *Ultrasound Med Biol.* 2017;43:2372—2394.
24. Malone AJ, Cournane S, Naydenova IG, Fagan AJ, Browne JE. Polyvinyl alcohol cryogel based vessel mimicking material for modelling the progression of atherosclerosis. *Phys Med.* 2020;69:1—8.
25. Van Prehn J, Schlösser FJ, Muhs BE, Verhagen HJ, Moll FL, Van Herwaarden JA. Oversizing of aortic stent grafts for abdominal aneurysm repair: a systematic review of the benefits and risks. *Eur J Vasc Endovasc Surg.* 2009;38:42—53.
26. Richards MS, Doyley MM. Non-rigid image registration based strain estimator for intravascular ultrasound elastography. *Ultrasound Med Biol.* 2013;39:515—533.
27. Arnaoutakis DJ, Sharma G, Blackwood S, et al. Strategies and outcomes for aortic endograft explantation. *J Vasc Surg.* 2019;69:80—85.
28. Kouvelos GN, Oikonomou K, Antoniou GA, Verhoeven EL, Katsargyris A. A systematic review of proximal neck dilatation after endovascular repair for abdominal aortic aneurysm. *J Endovasc Ther.* 2017;24:59—67.
29. Schlösser FJ, Gusberg RJ, Dardik A, et al. Aneurysm rupture after EVAR: can the ultimate failure be predicted? *Eur J Vasc Endovasc Surg.* 2009;37:15—22.
30. Prinssen M, Wever JJ, Mali WP, Eikelboom BC, Blankensteijn JD. Concerns for the durability of the proximal abdominal aortic aneurysm endograft fixation from a 2-year and 3-year longitudinal computed tomography angiography study. *J Vasc Surg.* 2001;33:S64—S69.
31. Monahan TS, Chuter TA, Reilly LM, Rapp JH, Hiramoto JS. Long-term follow-up of neck expansion after endovascular aortic aneurysm repair. *J Vasc Surg.* 2010;52:303—307.
32. Badran MF, Gould DA, Raza I, et al. Aneurysm neck diameter after endovascular repair of abdominal aortic aneurysms. *J Vasc Interv Radiol.* 2002;13:887—892.
33. Conners MS, Sternbergh WC, Carter G, Tonnessen BH, Yoselevitz M, Money SR. Endograft migration one to four years after endovascular abdominal aortic aneurysm repair with the AneuRx device: a cautionary note. *J Vasc Surg.* 2002;36:476—484.
34. Sampaio SM, Panneton JM, Mozes G, et al. Aortic neck dilation after endovascular abdominal aortic aneurysm repair: should oversizing be blamed? *Ann Vasc Surg.* 2006;20:338—345.
35. Mohan IV, Laheij RJ, Harris PL, Eurostar Collaborators. Risk factors for endoleak and the evidence for stent-graft oversizing in patients undergoing endovascular aneurysm repair. *Eur J Vasc Endovasc Surg.* 2001;21:344—349.
36. Petrik PV, Moore WS. Endoleaks following endovascular repair of abdominal aortic aneurysm: the predictive value of preoperative anatomic factors—a review of 100 cases. *J Vasc Surg.* 2001;33:739—744.
37. Dias NV, Resch T, Malina M, Lindblad B, Ivancev K. Intraoperative proximal endoleaks during AAA stent-graft repair: evaluation of risk factors and treatment with Palmaz stents. *J Endovasc Ther.* 2001;8:268—273.

38. Sampaio SM, Panneton JM, Mozes G, et al. AneuRx device migration: incidence, risk factors, and consequences. *Ann Vasc Surg.* 2005;19: 178—185.

39. Zarins CK, Bloch DA, Crabtree T, Matsumoto AH, White RA, Fogarty TJ. Stent graft migration after endovascular aneurysm repair: importance of proximal fixation. *J Vasc Surg.* 2003;38:1264—1272. discussion: 1272.

40. Kassab GS. Biomechanics of the cardiovascular system: the aorta as an illustratory example. *J R Soc Interface.* 2006;3:719—740.

41. Liu SQ. Influence of tensile strain on smooth muscle cell orientation in rat blood vessels. *J Biomech Eng.* 1998;120:313—320.

42. Wilkins H, Regelson W, Hoffmeister FS. The physiolgic importance of pulsatile blood flow. *N Engl J Med.* 1962;267:443—446.

43. Soroff HS, Many M, Birtwell WC, Giron F, Deterling RA. Hemodynamic effects of pulsatile and nonpulsatile blood flow. II. Selective depulsation of the aortic arch and brachiocephalic trunk. *Arch Surg.* 1969;98:321—325.